PROC. OF JSCE
No. 343, March 1984

ELASTIC-PLASTIC CONSTITUTIVE MODELS FOR THE BEHAVIOR OF SAND

By Hiroyoshi HIRAI, Eiji YANAGISAWA** and Masao SATAKE****

1. INTRODUCTION

The non-linear stress-strain relationships to predict the behavior of soils have been proposed. Based on the elastic-plastic modelling of soils and the associated flow rule, Roscoe, Schofield and Wroth[1] and Schofield and Wroth[2] developed an isotropic hardening modelling, called the Cam clay model. Modifying the Cam clay model by introducing another form of the dissipated energy, Burland[3] and Roscoe and Burland[4] propounded a constitutive relation called the Modified Cam clay model which possesses an elliptical yield surface. Recent theoretical investigations by Maier[5] and Zienkiewicz, Humphreson and Lewis[6] have suggested the uses of non-associated flow rule in which the yield function is not generally identical with the plastic potential. Lewin and Burland[7] and Wong and Mitchell[8] showed that the direction of the plastic strain increment vector does not generally hold normality to the yield surface of clay. Banerjee and Stipho[9] investigated the usefulness of the associated and non-associated flow rules by comparing with the experimental results of soft clay.

On the other hand, Rowe[10] proposed the stress-dilatancy relations for an assembly of particles based on a consideration of interaction between the spherical particles. Poorooshasb, Holubec and Sherbourne[11],[12] and Lade and Dunkan[13] showed the applicability of the non-associated flow rule through the deformation characteristics of sand in triaxial tests. Tatsuoka and Ishihara[14] investigated experimentally the yield locus of sand by employing different kinds of stress paths to suggest the usefulness of the non-associated flow rule. The experimental studies of sand and an assembly of particles in different three principal stresses were performed by Miyamori[15], Yamada and Ishihara[16] and Haruyama[17]. Mróz, Norris and Zeinkiewicz[18] propounded an anisotropic hardening model of soils, taking into account the anisotropic characteristics in plastic deformation. Based on the non-associated flow rule, Lade[19], Vermeer[20], Nishi and Esashi[21] and Molenkamp[22] proposed the double bardening models to predict the stress-strain relationships of sand adequately. The recent developments concerning the constitutive models of sand have been summarized in the book edited by Pande and Zienkiewicz[23]. According to several works mentioned above, it may be suggested that the yield surface of sand consists of a form such that the deviatoric stress at yielding increases as the mean principal stress increases, i.e., a shear yield locus and another form where the plastic volumetric strain is generated under isotropic stress state, i.e., a volumetric yield locus. In view of the experimental data by Ishihara and Okada[24] and Nishi[25], however, it may be suggested that the overconsolidated sand possesses an elliptical yield surface. Miura and Yamamoto[26] showed that the yield function of sand under high pressures may be represented by an elliptical surface. Therefore, it is posed as an important research to reconsider the shape of the yield function of sand.

In the present paper the seven constitutive models are proposed to investigate the applicability to describe the plastic behavior of sand properly. The stress-strain relations derived from these models are related to the associated and non-associated flow rules of incremental plasticity theory. The form of the yield function for sand is discussed through some experimental evidences in normally and lightly overconsolidated states. Effectiveness of these elastic-plastic constitutive models is studied by comparing with the experimental results of sand under triaxial compression and extension tests.

* Member of JSCE, Dr. Eng., Research Associate of Civil Engineering, Tohoku University.
** Member of JSCE, Dr. Eng., Professor of Civil Engineering, Tohoku University.
*** Member of JSCE, Dr. Eng., Professor of Civil Engineering, Tohoku University.

2. CONSTITUTIVE MODELS FOR SAND

Let us consider the general constitutive equation to describe the associated and non-associated flow rules synthetically. Since the normality of the plastic strain rate $\dot{E}_{ij}^{(p)}$ is assumed at a smooth point on the plastic potential g, we may write

$$\dot{E}_{ij}^{(p)}=\Lambda\frac{\partial g}{\partial T_{ij}} \quad \cdots\cdots(1)$$

where Λ is a function which depends on stress T_{ij}, stress rate and strain. Following the consistency condition given by Prager[27] and assuming the work-hardening parameter γ to be a function of plastic strain, we have the rate of yield function f in the form

$$\dot{f}=\frac{\partial f}{\partial T_{ij}}\dot{T}_{ij}+\frac{\partial f}{\partial E_{ij}^{(p)}}\dot{E}_{ij}^{(p)}+\frac{\partial f}{\partial \gamma}\frac{\partial \gamma}{\partial E_{ij}^{(p)}}\dot{E}_{ij}^{(p)}=0 \quad \cdots\cdots(2)$$

This means that loading from a plastic state must lead to another plastic state. Substituting Eq. (1) into Eq. (2) and solving for Λ, we obtain

$$\dot{E}_{ij}^{(p)}=h\frac{\partial g}{\partial T_{ij}}\frac{\partial f}{\partial T_{kl}}\dot{T}_{kl} \quad \cdots\cdots(3)$$

where

$$h=-1\Big/\left(\frac{\partial f}{\partial E_{mn}^{(p)}}+\frac{\partial f}{\partial \gamma}\frac{\partial \gamma}{\partial E_{mn}^{(p)}}\right)\frac{\partial g}{\partial T_{mn}} \quad \cdots\cdots(4)$$

Eq. (3) is the same form as the relation given by Hill[28].

Koiter[29] showed that if yield functions act independently, the total plastic deformation can be written as a sum of contributions from some of yield functions. Applying the method given by Koiter to Eq. (3), we can write

$$\dot{E}_{ij}^{(p)}=\sum_{p=1}^{k}C_p h_p\frac{\partial g_p}{\partial T_{ij}}\frac{\partial f_p}{\partial T_{kl}}\dot{T}_{kl} \quad \cdots\cdots(5)$$

where

$$h_p=-1\Big/\left(\frac{\partial f_p}{\partial E_{mn}^{(p)}}+\frac{\partial f_p}{\partial \gamma_p}\frac{\delta \gamma_p}{\partial E_{mn}^{(p)}}\right)\frac{\delta g_p}{\partial T_{mn}}$$

p not summed $\cdots\cdots(6)$

$$C_p=0 \quad \text{if} \quad f_p<0 \quad \text{or} \quad (\partial f_p/\partial T_{ij})\dot{T}_{ij}<0 \quad \cdots\cdots(7)$$

$$C_p=1 \quad \text{if} \quad f_p=0 \quad \text{and} \quad (\partial f_p/\partial T_{ij})\dot{T}_{ij}\geqq 0 \quad \cdots\cdots(8)$$

and where f_p is a yield function, g_p is a plastic potential and γ_p is a work-hardening parameter. Since the plastic potential g_p is assumed to be generally different from the yield function f_p in Eq. (5), Eq. (5) with Eqs. (6) to (8) represents a form of non-associated flow rule.

The yield functions, plastic potentials and work-hardening parameters used in the seven soil models proposed in the present paper are summarized in **Table 1**. Especially the models (d) and (f) are illustrated in **Figs. 1-1** and **1-2** respectively. The associated flow rule based on the Modified Cam clay model[3),4)] is applied to the

Table 1 Yield functions, plastic potentials and work-hardening parameters used in the seven soil models.

Models	Yield Functions	Plastic Potentials	Work-Hardening Parameters
(a)	$f_1=J_2+\beta I_1^2+\gamma_1 I_1=0$	$g_1=J_2+\beta I_1^2+\gamma_1 I_1=0$	$\dot{\gamma}_1=\phi_1 T_{ii}\dot{E}_{jj}^{(p)}/3+\phi_2 T'_{ij}\dot{E}_{ij}^{(p)}$
(b)	$f_1=J_2+\beta I_1^2+\gamma_1 I_1=0$	$g_1=\sqrt{J_2}/I_1-M\ln\lvert I_1/I_0\rvert=0$	$\dot{\gamma}_1=\phi_1 T_{ii}\dot{E}_{jj}^{(p)}/3+\phi_2 T'_{ij}\dot{E}_{ij}^{(p)}$
(c)	$f_1=J_2+\beta I_1^2+\gamma_1 I_1=0$ $f_2=\sqrt{J_2}+\eta I_1+\gamma_2=0$	$g_1=\sqrt{J_2}/I_1-M\ln\lvert I_1/I_0\rvert=0$ $g_2=\sqrt{J_2}+\eta I_1+\gamma_2=0$	$\dot{\gamma}_1=\phi_1 T_{ii}\dot{E}_{jj}^{(p)}/3+\phi_2 T'_{ij}\dot{E}_{ij}^{(p)}$ $\dot{\gamma}_2=\psi_1 T_{ii}\dot{E}_{jj}^{(p)}/3+\psi_2 T'_{ij}\dot{E}_{ij}^{(p)}$
(d)	$f_1=I_1+\gamma_1=0$ $f_2=J_2+\gamma_2 I_1=0$	$g_1=I_1+\gamma_1=0$ $g_2=\sqrt{J_2}/I_1-M\ln\lvert I_1/I_0\rvert=0$	$\dot{\gamma}_1=\phi_1 T_{ii}\dot{E}_{jj}^{(p)}/3$ $\dot{\gamma}_2=\psi_1 T_{ii}\dot{E}_{jj}^{(p)}/3+\psi_2 T'_{ij}\dot{E}_{ij}^{(p)}$
(e)	$f_1=J_2+\beta I_1^2+\gamma_1 I_1=0$ $f_2=J_2+\gamma_2 I_1=0$	$g_1=\sqrt{J_2}/I_1-M\ln\lvert I_1/I_0\rvert=0$ $g_2=\sqrt{J_2}/I_1-M\ln\lvert I_1/I_0\rvert=0$	$\dot{\gamma}_1=\phi_1 T_{ii}\dot{E}_{jj}^{(p)}/3+\phi_2 T'_{ij}\dot{E}_{ij}^{(p)}$ $\dot{\gamma}_2=\psi_1 T_{ii}\dot{E}_{jj}^{(p)}/3+\psi_2 T'_{ij}\dot{E}_{ij}^{(p)}$
(f)	$f_1=I_1+\gamma_1=0$ $f_2=J_2+\beta I_1^2+\gamma_2 I_1=0$	$g_1=I_1+\gamma_1=0$ $g_2=\sqrt{J_2}/I_1-M\ln\lvert I_1/I_0\rvert=0$	$\dot{\gamma}_1=\phi_1 T_{ii}\dot{E}_{jj}^{(p)}/3$ $\dot{\gamma}_2=\psi_1 T_{ii}\dot{E}_{jj}^{(p)}/3+\psi_2 T'_{ij}\dot{E}_{ij}^{(p)}$
(g)	$f_1=J_2+\beta I_1^2+\gamma_1 I_1=0$ $f_2=J_2+\gamma_2 I_1=0$ $f_3=I_1+\gamma_3=0$	$g_1=\sqrt{J_2}/I_1-M\ln\lvert I_1/I_0\rvert=0$ $g_2=\sqrt{J_2}/I_1-M\ln\lvert I_1/I_0\rvert=0$ $g_3=I_1+\gamma_3=0$	$\dot{\gamma}_1=\phi_1 T_{ii}\dot{E}_{jj}^{(p)}/3+\phi_2 T'_{ij}\dot{E}_{ij}^{(p)}$ $\dot{\gamma}_2=\psi_1 T_{ii}\dot{E}_{jj}^{(p)}/3+\psi_2 T'_{ij}\dot{E}_{ij}^{(p)}$ $\dot{\gamma}_3=\phi_3 T_{ii}\dot{E}_{jj}^{(p)}/3$

Notation: I_0 is a work-hardening parameter.

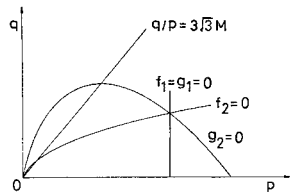

Fig. 1-1 Model (d).

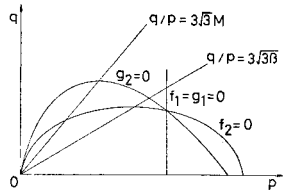

Fig. 1-2 Model (f).

model (a). For the model (b), the yield function used in the Modified Cam clay model and the plastic potential employed in the Cam clay model[1] are adopted. The yield function f_2 and plastic potential g_2 in the model (c) are the same forms proposed by Drucker and Prager[30]. The model (d) is similar to the double hardening model, which consists of shear and volumetric yield loci, proposed by Vermeer[20] and Nishi and Esashi[21]. The yield function f_2 in the model (d) is assumed under the low effective mean principal stress on the basis of the experimental data presented by Tatsuoka and Ishihara[14]. The model (e) made up of elliptical and parabolic yield surfaces bears resemblance to the models where Lade[19] and Molenkamp[22] employ conical and spherical yield functions. The model (f) is an extension of the model (b) because, in the model (f), another yield function f_1 is adopted besides the yield function f_2. The model (g) is considered to be a combination of the models (d) and (f) and is an extension of the model (e).

Assuming that the work-hardening parameter may depend not only on the plastic work related with the change in volume but also on that related with the change in shape, Hirai and Satake[31] proposed the rate of the work-hardening parameter in the form shown in **Table 1**.

Substitution of yield functions, plastic potentials and work-hardening parameters for each model into Eq. (5) leads to the following seven stress-strain relationships:

For the model (a)

$$\dot{E}_{ij}^{(p)}=-C_1\frac{\dot{J}_2+(\beta I_1-J_2/I_1)\dot{I}_1}{\{(2\phi_2-\phi_1)J_2+\beta\phi_1 I_1^2\}I_1}\times\left\{T_{ij}'+\left(\beta I_1-\frac{J_2}{I_1}\right)\delta_{ij}\right\} \quad \cdots\cdots(9)$$

where $\dot{J}_2$ and $\dot{I}_1$ are rates of the invariants $J_2=T_{ij}'T_{ij}'/2$ and $I_1=T_{ii}$ respectively, T_{ij}' is the deviatoric stress and δ_{ij} is called the Kronecker delta.

For the model (b)

$$\dot{E}_{ij}^{(p)}=-C_1\frac{\dot{J}_2+(\beta I_1-J_2/I_1)\dot{I}_1}{\{(\phi_2-\phi_1)\sqrt{J_2}-M\phi_1 I_1\}I_1}\times\left\{\frac{T_{ij}'}{2\sqrt{J_2}}-\left(\frac{\sqrt{J_2}}{I_1}+M\right)\delta_{ij}\right\} \quad \cdots\cdots(10)$$

For the model (c)

$$\dot{E}_{ij}^{(p)}=-C_1\frac{\dot{J}_2+(\beta I_1-J_2/I_1)\dot{I}_1}{\{(\phi_2-\phi_1)\sqrt{J_2}-M\phi_1 I_1\}I_1}\times\left\{\frac{T_{ij}'}{2\sqrt{J_2}}-\left(\frac{\sqrt{J_2}}{I_1}+M\right)\delta_{ij}\right\}-C_2\frac{\dot{J}_2/(2\sqrt{J_2})+\eta\dot{I}_1}{(\eta\phi_1 I_1+\phi_2\sqrt{J_2})}\left(\frac{T_{ij}'}{2\sqrt{J_2}}+\eta\delta_{ij}\right) \quad \cdots\cdots(11)$$

For the model (d)

$$\dot{E}_{ij}^{(p)}=-C_1\frac{1}{\phi_1}\frac{\dot{I}_1}{I_1}\delta_{ij}-C_2\frac{\dot{J}_2-(J_2/I_1)\dot{I}_1}{\{(\phi_2-\phi_1)\sqrt{J_2}-M\phi_1 I_1\}I_1}\times\left\{\frac{T_{ij}'}{2\sqrt{J_2}}-\left(\frac{\sqrt{J_2}}{I_1}+M\right)\delta_{ij}\right\} \quad \cdots\cdots(12)$$

For the model (e)

$$\dot{E}_{ij}^{(p)}=-\left[C_1\frac{\dot{J}_2+(\beta I_1-J_2/I_1)\dot{I}_1}{\{(\phi_2-\phi_1)\sqrt{J_2}-M\phi_1 I_1\}}+C_2\frac{\dot{J}_2-(J_2/I_1)\dot{I}_1}{\{(\phi_2-\phi_1)\sqrt{J_2}-M\phi_1 I_1\}}\right]\times\frac{1}{I_1}\left\{\frac{T_{ij}'}{2\sqrt{J_2}}-\left(\frac{\sqrt{J_2}}{I_1}+M\right)\delta_{ij}\right\} \quad \cdots\cdots(13)$$

For the model (f)

$$\dot{E}_{ij}^{(p)}=-C_1\frac{1}{\phi_1}\frac{\dot{I}_1}{I_1}\delta_{ij}-C_2\frac{\dot{J}_2+(\beta I_1-J_2/I_1)\dot{I}_1}{\{(\phi_2-\phi_1)\sqrt{J_2}-M\phi_1 I_1\}I_1}\times\left\{\frac{T_{ij}'}{2\sqrt{J_2}}-\left(\frac{\sqrt{J_2}}{I_1}+M\right)\delta_{ij}\right\} \quad \cdots\cdots(14)$$

For the model (g)

$$\dot{E}_{ij}^{(p)}=-\left[C_1\frac{\dot{J}_2+(\beta I_1-J_2/I_1)\dot{I}_1}{\{(\phi_2-\phi_1)\sqrt{J_2}-M\phi_1 I_1\}}+C_2\frac{\dot{J}_2-(J_2/I_1)\dot{I}_1}{\{(\phi_2-\phi_1)\sqrt{J_2}-M\phi_1 I_1\}}\right]\times\frac{1}{I_1}\left\{\frac{T_{ij}'}{2\sqrt{J_2}}-\left(\frac{\sqrt{J_2}}{I_1}+M\right)\delta_{ij}\right\}-C_3\frac{1}{\phi_3}\frac{\dot{I}_1}{I_1}\delta_{ij} \quad \cdots\cdots(15)$$

In Eqs. (9) to (15), M, β, η, ϕ_1, ϕ_2, ϕ_3, ϕ_1 and ϕ_2 denote material constants.

3. TESTING APPARATUS AND SPECIMENS

The material used in the present investigation is Toyoura Sand, which properties are given in **Fig. 2** and **Table 2**. The sample was in the form of a cylinder 12.5 cm in length by 5 cm in diameter. The samples were prepared by pouring oven-dried sand into a split mold filled with de-aired water, being compacted by tapping the side wall of the mold by a wooden hammer. The average void ratio and the average relative density of samples obtained by use of the method above are 0.76 and 59.3% respectively. After each specimen was set up in the cell with 4.9 kPa vacuum, the cell pressure was raised to 9.8 kPa. Then, the cell pressure was increased up to a desired value in the isotropic stress condition and the consolidation duration was specified to be two hours. The back pressure of 98 kPa was supplied to all specimens. All tests performed in the present paper were under the drained condition and were loaded by the stress control. Since the volume change measured in burette is generally subjected to errors due to the penetration of rubber membrane into interstices between sand particles under the application of the cell pressure, this error was corrected by use of the membrane penetration calibration test methods (e.g., Moroto[32]).

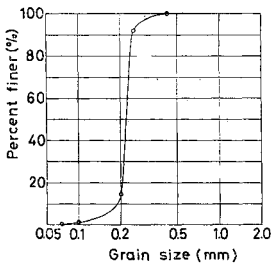

Fig. 2 Grain size distribution of the sand.

Table 2 Physical properties of sand used in the present study.

Specific Gravity of Solids	$G_s=2.65$
Maximum Void Ratio	$e_{max}=0.99$
Minimum Void Ratio	$e_{min}=0.61$
Uniformity Coefficient	$U_c=1.31$
Effective Grain Size	D_{10}(mm)$=0.18$

4. PREDICTED AND OBSERVED RESPONSES OF SAND FOR TRIAXIAL STRESS STATES

Let us investigate the usefulness of the seven soil models proposed in the section 2 through the experimental data of sand. The axisymmetric triaxial tests are carried out and the effective axial stress σ_1 and the effective radial stresses $\sigma_2=\sigma_3$ are supplied. The effective mean principal stress $p=(\sigma_1+2\sigma_3)/3$ and the axial difference stress $q=|\sigma_1-\sigma_3|$ are used. For strains in the triaxial tests, the volumetric strain $v=e_1+2e_3$ and the deviatoric strain $d=2/3|e_1-e_3|$ are adopted, where e_1 is the strain in the axial direction and e_3 is that in the radial direction. The compressive stresses and strains are taken to be positive. In the triaxial tests, it is seen that $J_2=q^2/3$ and $I_1=-3p$.

(1) Experimental Results

In order to divide the plastic strain from the total strain, the elastic moduli will be determined through experimental data. The elastic shear modulus G is determined from unloading and reloading curves in the relation between q and d as follows:

$$G=95.8\,\text{MPa} \quad \cdots\cdots(16)$$

The rate of the volumetric elastic strain v^e is given by

$$\dot{v}^e=\kappa\dot{p}/p \quad \cdots\cdots(17)$$

where κ is the slope of the compression line. From the swelling and recompressing lines in the relation between p and v it is found that

$$\kappa=6.34\times10^{-4} \quad \cdots\cdots(18)$$

Fig. 3 shows the relationships between the ratio of plastic strain rates $\dot{v}^p/\dot{d}^p$ and the ratio of stresses q/p for triaxial compression tests specified by the stress paths A, B, C, D, E, F and G in **Fig. 3**. **Fig. 4** shows the relationships between the ratio of plastic strain rates $\dot{v}^p/\dot{d}^p$ and the ratio of stresses q/p for triaxial extension tests designated by the stress paths A, B, C, D, E and F in **Fig. 4**. In order to investigate whether the plastic potentials employed in the present paper are applicable to the description of stress-strain relationships of sand, the experimental data shown in **Figs. 3** and **4** will be used.

Fig. 5 and **6** show the relationships between the deviatoric plastic strain d^p and the ratio of stresses q/p and those between the volumetric plastic strain v^p and the ratio of stresses q/p concerning four stress paths of A, B, C and D in **Fig. 3** for the triaxial compression tests. **Figs. 7** and **8** show the relationships between the deviatoric plastic strain d^p and the ratio of stresses q/p and those between the volumetric plastic strain v^p and q/p concerning four stress paths of A, B, C and D in **Fig. 4** for the triaxial extension tests. The experimental results shown in **Figs. 5** to **8** will be employed to determine the material

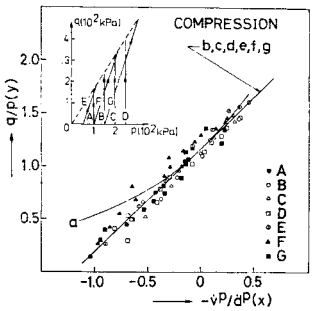

Fig. 3 Relationships between $\dot{v}^p/\dot{d}^p$ and q/p for triaxial compression tests.

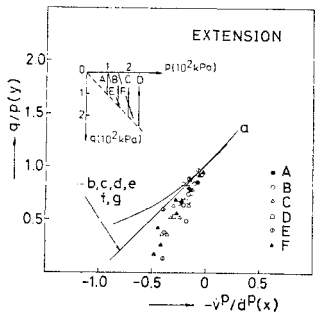

Fig. 4 Relationships between $\dot{v}^p/\dot{d}^p$ and q/p for triaxial extension tests.

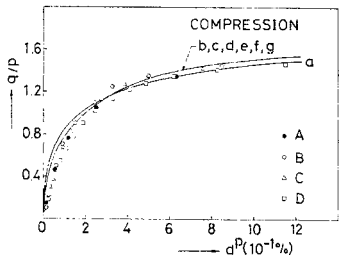

Fig 5 Relationships between q/p and d^p for constant-p compression tests.

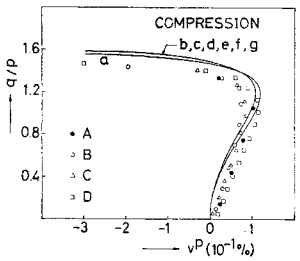

Fig. 6 Relationships between q/p and v^p for constant-p compression tests.

constants in the work-hardening parameters.

Fig. 9 represents stress paths A, B, C, D, E, F, G, H and I where the constant-q compression

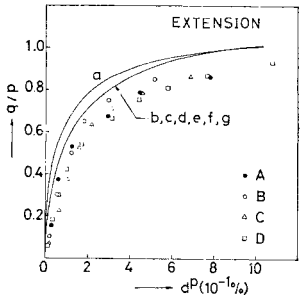

Fig. 7 Relationships between q/p and d^p for constant-p extension tests.

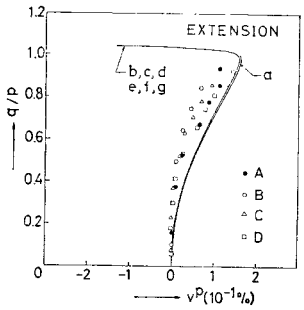

Fig. 8 Relationships between q/p and v^p for constant-p extension tests.

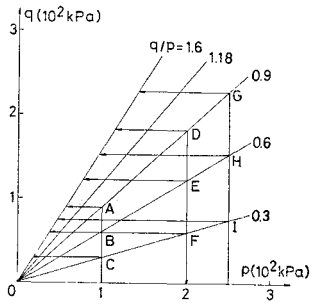

Fig. 9 Constant-q stress paths subsequent to constant-p compression tests.

tests are continued after the constant-p compression tests have been finished concerning three kinds of the initial stress p, 98 kPa, 196 kPa and 245 kPa, and three kinds of the ratio of stresses q/p, 0.3, 0.6 and 0.9. In order to verify whether the shapes of yield functions employed in the seven soil models are relevant to the description of the plastic behavior of sand, the experiments with the stress paths illustrated in **Fig. 9** were performed. **Figs. 10** and **12** show the relationships between the deviatoric plastic strain defined as $\bar{d}^p=2/3(e_1^p-e_3^p)$ and the ratio of stresses q/p for the part of constant-q compression tests in **Fig. 9**. **Figs. 11** and **13** show the relationships be-

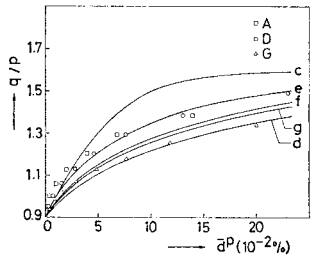

Fig. 10 Relationships between q/p and $\bar{d}^p$ for constant-q compression tests.

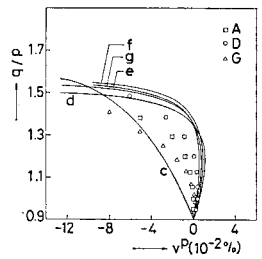

Fig. 11 Relationships between q/p and v^p for constant-q compression tests.

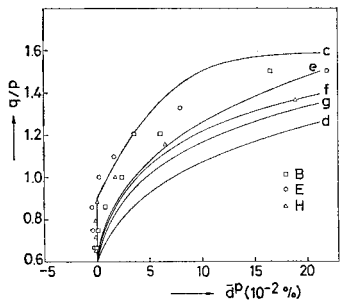

Fig. 12 Relationships between q/p and $\bar{d}^p$ for constant-q compression tests.

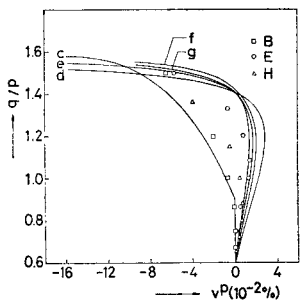

Fig. 13 Relationships between q/p and v^p for constant-q compression tests.

tween the volumetric plastic strain v^p and the ratio of stresses q/p for the part of constant-q compression tests in **Fig. 9**. It is found from **Figs. 10** to **13** that the stress-strain relationships for a constant-q test have the trend similar to those in another constant-q test after being subjected to the same ratio of stresses q/p irrespective of the magnitude of initial mean principal stress p.

(2) Model (a)

Let us determine the material constants β, ϕ_1 and ϕ_2 in Eq. (9) for the model (a) through experimental results. By use of Eq. (9), the following relation is obtained in triaxial tests:

$$x=(y-27\beta/y)/2 \quad \cdots\cdots(19)$$

where $x=-\dot{v}^p/\dot{d}^p$, $y=q/p$, $\dot{v}^p$ and $\dot{d}^p$ are rates of volumetric and deviatoric plastic strains and Eq. (19) is first proposed by Burland[3] and Roscoe and Burland.[4] In the triaxial constant-p tests, the following relations are obtained from Eq. (9):

$$\left.\begin{aligned}\dot{d}^p/\dot{y}&=4y^2/[9\phi_1\{27\beta+(2n-1)y^2\}]\\ \dot{v}^p/\dot{y}&=2(27\beta-y^2)y/[9\phi_1\{27\beta+(2n-1)y^2\}]\end{aligned}\right\} \quad \cdots\cdots(20)$$

where $n=\phi_2/\phi_1$. Applying the data in **Figs. 3** to **8** for triaxial tests to Eqs. (19) and (20), we have

$$\left.\begin{aligned}&\beta_c=0.052, \quad \beta_e=0.037\\ &\phi_{1c}=81.6, \quad \phi_{1e}=55.8\\ &n_c=0.228, \quad n_e=0.047\end{aligned}\right\} \quad \cdots\cdots(21)$$

where β_c, ϕ_{1c} and n_c and β_e, ϕ_{1e} and n_e are β, ϕ_1 and n for triaxial compression and extension tests respectively. It is seen from **Figs. 3** to **8** that the theoretical stress-strain relationships of Eqs. (19) and (20) with Eq. (21), denoted by the curves ***a*** predict the experimental results fairly well when monotonous increasing loads are supplied in triaxial compression and extension tests.

(3) Model (b)

Let us consider the material constants M, ϕ_1, ϕ_2 and β contained in the stress-strain relationship given by Eq. (10) for the model (b). It is found from Eq. (10) that

$$x=y-3\sqrt{3}M \quad \cdots\cdots(22)$$

In the triaxial constant-p tests, the following relations are derived from Eq. (10):

$$\left.\begin{aligned}\dot{d}^p/\dot{y}&=2y/[9\sqrt{3}\,\phi_1\{3M+(n-1)y/\sqrt{3}\}]\\ \dot{v}^p/\dot{y}&=2y\{M-y/(3\sqrt{3})\}/\\ &\qquad [3\phi_1\{3M+(n-1)y/\sqrt{3}\}]\end{aligned}\right\} \quad \cdots\cdots(23)$$

Applying the data in **Figs. 3** to **8** to Eqs. (22) and (23), we get

$$\left.\begin{aligned} &M_c=0.228, \quad M_e=0.192 \\ &\phi_{1c}=86.9, \quad \phi_{1e}=56.4 \\ &n_c=0.25, \quad n_e=0.05 \end{aligned}\right\} \cdots\cdots\cdots\cdots\cdots\cdots (24)$$

If the phase transformation line[24] given by $q/p=3\sqrt{3}M$ for the plastic potential is assumed to be identical with the line $q/p=3\sqrt{3\beta}$ for the yield function, by use of Eq. (24), we find

$$\beta_c=0.052, \quad \beta_e=0.037 \cdots\cdots\cdots\cdots\cdots\cdots (25)$$

The theoretical relationships Eqs. (22) and (23) with Eq. (24) correspond to the curves ***b*** in **Figs. 3** to **8**. Comparing the curves ***a*** and ***b*** in **Figs. 3** to **8**, we may see that the curves ***b*** of Eqs. (22) and (23) based on the non-associated flow rule can predict the experimental results better than the curves ***a*** of Eqs. (19) and (20) on the basis of the associated flow rule. This is the reason why the non-associated flow rule is adopted in the other models except the model (a).

(4) Models (c), (d), (e) and (g)

The deviatoric and volumetric plastic strains do occur on the constant-q compression stress paths in **Fig. 9**, as shown in **Figs. 10** to **13**. This may suggest that the models (a) and (b) are not necessarily relevant to the description of plastic deformation of sand since the plastic strains are supposed to not appear inside of the yield functions. As it is necessary to improve the models (a) and (b), then the models (c), (d), (e), (f) and (g) are proposed to describe the plastic behavior in constant-q tests as well as the constant-p tests properly.

By use of the method similar to the derivation made in the models (a) and (b), it is easy to determine the values of material constants in the constitutive relations, (11), (12), (13) and (15). The stress-strain cnrves, ***c***, ***d***, ***e*** and ***g*** shown in **Figs. 3** to **13** are obtained from the equations (11), (12), (13) and (15) respectively.

(5) Model (f)

The initial and subsequent yield functions f_2 in the model (f) for a constant-p stress path and failure and phase transformation lines are shown in **Fig. 14**. Three subsequent yield loci in **Fig. 14** correspond to the cases for the ratio of stresses $q/p=0.3$, 0.6 and 0.9. For a constant-q test shown in **Fig. 9**, a yield surface given by f_2 begins to expand from the point where the constant-p tests has been finished as the ratio of stresses q/p increases.

Recent experimental studies by Tatsuoka and Ishihara[14], Ishihara and Okada,[24] Miura and Yamamoto[26] and Nishi[25] have suggested that the shape of the yield function for sand may be

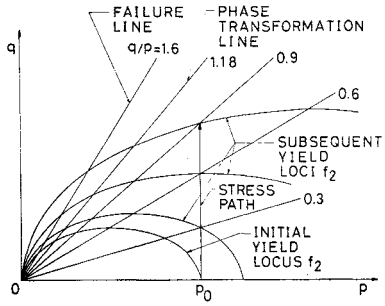

Fig. 14 Initial and subsequent yield loci for the constant-p stress path, failure and phase transformation lines.

assumed to be an elliptical surface. As far as the material constants β and M in **Fig. 1-2** for the triaxial compression tests are concerned, the following values are obtained for the loosely compacted sands tested by workers above:

$\beta_c=9.25\times10^{-3}$		from 14)
$\beta_c=1.16\times10^{-2}$,	$M_c=0.24$	from 24)
$\beta_c=2.03\times10^{-2}$,	$M_c=0.25$	from 26)
$\beta_c=1.66\times10^{-2}$,	$M_c=0.212$	from 25)

Although the experiment for overconsolidated sand was not performed in the present paper, it is assumed that the material constant β for triaxial compression tests in the yield function $f_2=0$ takes

$$\beta_c=1.33\times10^{-2} \cdots\cdots\cdots\cdots\cdots\cdots (26)$$

since the ratio of stresses $q/p=3\sqrt{3\beta}$, as shown in **Fig. 1-2**, at the top of the yield function $f_2=0$ may be assumed approximately to be 0.6 for the present in the light of the experimental results given by the researchers above. As Eqs. (10) and (14) are reduced to the identical relation in the constant-p tests, the material constants M, ϕ_1 and $m=\phi_2/\phi_1$ in Eq. (14) are same as M, ϕ_1 and n in Eq. (24) respectively.

In the case of constant-q tests shown in **Fig. 9**, the following relations are obtained from Eq. (14):

$$\left.\begin{aligned} &\dot{d}^p/\dot{y}=(y^2/9-3\beta)/\\ &\qquad [\sqrt{3}\,y\{3M+(m-1)y/\sqrt{3}\}\phi_1] \\ &\dot{v}^p/\dot{y}=3(y^2/9-3\beta)\{M-y/(3\sqrt{3})\}/\\ &\qquad [y\{3M+(m-1)y/\sqrt{3}\}\phi_1] \end{aligned}\right\} \cdots\cdots\cdots\cdots\cdots\cdots (27)$$

The curves ***f*** in **Figs. 3** to **13** show Eq. (14) and it is found that the predicted curves ***f*** can describe the observed results properly.

(6) Stress-Strain Relationships in General Triaxial Stress States

In view of the results obtained in the previous sections, the four models (d), (e), (f) and (g) are capable of predicting many of the observed features of plastic behavior of sand adequately. In particular, since it may be noticed that the soil model (f), made by a simple and reasonable combination of yield functions and plastic potentials, is able to describe the experimental data properly, the attention is focussed on Eq. (14) for the model (f) in what follows.

Let us consider the stress-strain relationship of Eq. (14) in the case of the general stress state. The equivalent plastic strain rate $\dot{\varepsilon}^p$ is defined in the form[28]

$$\dot{\varepsilon}^p=\{2/3\dot{E}_{ij}{}'^{(p)}\dot{E}_{ij}{}'^{(p)}\}^{1/2} \quad \cdots\cdots(28)$$

The equivalent stress σ is expressed by the second invariant of the deviatoric stress in the form[28]

$$\sigma=\{3J_2\}^{1/2} \quad \cdots\cdots(29)$$

By use of Eqs. (28) and (29), the relationship between the equivalent plastic strain and the ratio of the equivalent stress to the first invariant of stress in the case of constant-I_1 tests is derived from Eq. (14) as follows:

$$\dot{\varepsilon}^p/\dot{z}=2z/[3\{(m-1)z+\sqrt{3}M\}\phi_1] \quad \cdots\cdots(30)$$

where $z=\sigma/I_1{}^*$ and $I_1{}^*=\sigma_1+\sigma_2+\sigma_3$. Integrating Eq. (30) with respect to z leads to

$$\varepsilon^p=\frac{2}{3(m-1)\phi_1}\left[z+\frac{\sqrt{3}M}{1-m}\times\ln\left\{\frac{\sqrt{3}M-(1-m)z}{\sqrt{3}M}\right\}\right] \quad \cdots\cdots(31)$$

From Eqs. (14) and (29), the relationship between the volumetric plastic strain v^p and the ratio of the equivalent stress to the first invariant of stress $\sigma/I_1{}^*$ is represented for the constant-I_1 tests in the following form

$$\dot{v}^p/\dot{z}=2z(\sqrt{3}M-z)/[\{(m-1)z+\sqrt{3}M\}\phi_1] \quad \cdots\cdots(32)$$

Integration of Eq. (32) with respect to z leads to

$$v^p=\frac{2}{(m-1)\phi_1}\left[-\frac{z^2}{2}+\frac{\sqrt{3}Mm}{m-1}z-\frac{3M^2m}{(1-m)^2}\times\ln\left\{\frac{\sqrt{3}M-(1-m)z}{\sqrt{3}M}\right\}\right] \quad \cdots\cdots(33)$$

For the parameters M, ϕ_1 and m in Eqs. (31) and (33), M, ϕ_1 and n in Eq. (24) are used for triaxial compression and extension tests. In view of data presented by Miyamori[15], Yamada and Ishihara[16] and Haruyama[17], it may be suggested that the parameters M, ϕ_1 and m for triaxial compression tests take maximum values and those for triaxial extension ones have minimum values in genuine

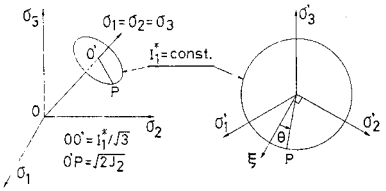

Fig. 15 Stress state in stress space and on π-plane.

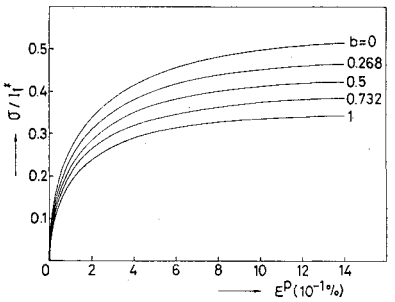

Fig. 16 Relationships between $\sigma/I_1{}^*$ and ε^p for b-values.

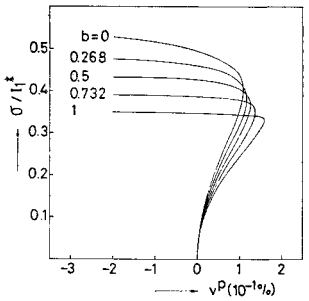

Fig. 17 Relationships between $\sigma/I_1{}^*$ and v^p for b-values.

triaxial tests. Subsequently, for the parameters M, ϕ_1 and m in the general stress conditions, it may be assumed simply that[33]

$$M=(M_e-M_c)b+M_c \quad \cdots\cdots(34)$$

$$\phi_1=(\phi_{1e}-\phi_{1c})b+\phi_{1c} \quad \cdots\cdots(35)$$

$$m=(m_e-m_c)b+m_c \quad \cdots\cdots(36)$$

where

$$b=(\sigma_2-\sigma_3)/(\sigma_1-\sigma_3) \quad \cdots\cdots(37)$$

$$\sqrt{3}\tan\theta=(2\sigma_2-\sigma_1-\sigma_3)/(\sigma_1-\sigma_3)=2b-1 \quad \cdots\cdots(38)$$

and where σ_1, σ_2 and σ_3 are the major, intermediate and minor principal stresses respectively, the anti-clockwise direction θ is measured from the ξ-axis perpendicular to σ_2'-axis, as shown in **Fig. 15.** **Fig. 15** shows a stress state in three principal stresses σ_1, σ_2 and σ_3 and the stress

state can be designated by invariants I_1 and J_2 and the angle θ on π-plane (I_1=const.), where σ_1', σ_2' and σ_3' are the deviatoric principal stresses. Eqs. (34) to (36) mean that the parameters M, ψ_1 and m are functions of b-value, which represents the stress state on π-plane. If a stress path is specified by b-value, the material constants M, ψ_1 and m are fixed by Eqs. (34) to (36) respectively. Although the stress path in a general elastic-plastic problem is changed from point to point in stress space, the parameters M, ψ_1 and m are dependent on only the b-value.

Substituting Eqs. (34) to (36) into Eq. (31), we obtain the relationship between the equivalent plastic strain ε^p and the ratio of stresses σ/I_1^* for several b-values, as shown in **Fig. 16**. Substitution of Eqs. (34) to (36) into Eq. (33) leads to the relationship between the volumetric plastic strain v^p and the ratio of stresses σ/I_1^* for various b-values, as shown in **Fig. 17**. As the b-value increases from zero to one, the slope of the stress-strain curve for each b-value becomes gentle in the range of small strain and the failure stress decreases gradually, as seen in **Figs. 16** and **17**. This trend is same as the experimental data given by Miyamori[15], Yamada and Ishihara[16] and Haruyama[17]. Therefore, it is considered that the theoretical relations Eqs. (31) and (33) may predict properly the stress-strain relationships for various b-values in the case of constant-I_1 tests.

5. CONCLUSIONS

Several important results in the present paper are summarized as follows:

(1) The seven soil models consisting of yield function, work-hardening parameter and plastic potential have been proposed in order to investigate the capability of predicting the plastic behavior of sand.

(2) The incremental stress-strain relationships for the seven models have been derived on the basis of associated and non-associated theories of incremental plasticity.

(3) Effectiveness of these stress-strain relations has been evaluated by comparing with the experimental results for triaxial compression and extension tests.

(4) The non-associated flow rule gives better predictions than the associated flow rule.

(5) The four soil models (d), (e), (f) and (g) in the present paper can predict many of the observed features of plastic behavior of sand fairly well.

(6) Above all, the model (f), supported by experimental evidences found in studies by several workers, possesses a simple and reasonable combination of yield functions and plastic potentials and is able to describe the experimental data adequately.

(7) The stress-strain relationships in three different principal stresses are obtained on the basis of the assumption that the material constants in yield functions and plastic potentials are dependent on only the b-value.

REFERENCES

1) Roscoe, K. H., A. N. Schofield and C. P. Wroth: On the yielding of soils, Geotechnique, Vol. 8, pp. 22～53, 1958.
2) Schofield, A. N. and C. P. Wroth: Critical State Soil Mechanics, McGraw-Hill, London, 1968.
3) Burland, J. B.: The yielding and dilatation of clay, Correspondence, Geotechnique, Vol. 15, pp. 211～214, 1965.
4) Roscoe, K. H. and J. B. Burland: On the generalized stress-strain behaviour of "wet" clay, in Engineering Plasticity, ed. Heyman J. and F. A. Leckie, Cambridge University Press, pp. 535～609, 1968.
5) Maier, G.: A minimum principal for incremental elasto-plasticity with non-associated flow laws, Journal of the Mechanics and Physics of Solids, Vol. 18, pp. 319～330, 1970.
6) Zienkiewicz, O. C., C. Humphreson and R. Lewis, Associated and non-associated viscoplasticity and plasticity in soil mechanics, Geotechnique, Vol. 25, pp. 671～689, 1975.
7) Lewin, P. I. and J. B. Burland: Stress probe experiments on saturated normally consolidated clay, Geotechnique, Vol. 20, pp. 38～56, 1970.
8) Wong, P. K. and R. J. Mitchell: Yielding and plastic flow of sensitive cemented clay, Geotechnique, Vol. 25, pp. 763～782, 1975.
9) Banerjee, P. K. and A. S. Stipho: Associated and non-associated constitutive relations for undrained behaviour of isotropic soft clays, International Journal for Numerical and Analytical Methods in Geomechanics, Vol. 2, pp. 35～56, 1978.
10) Rowe, P. W.: The stress-dilatancy relation for static equilibrium of an assembly of particles in contact, Proceedings of the Royal Society of London, Ser, A. Vol. 269, pp. 500～527, 1962.
11) Poorooshasb, H. B., I. Holubec and A N. Sherbourne: Yielding and flow of sand in triaxial compression, Part I, Canadian Geotechnical Journal, Vol. 3, No. 4, pp. 179～190, 1966.
12) Poorooshasb, H. B., I. Holubec and A. N. Sherbourne: Yielding and flow of sand in triaxial compression, Parts II and III, Canadian Geotechnical Journal, Vol. 4, No. 4, pp. 377～398, 1967.
13) Lade, P. V. and J. M. Duncan: Elastoplastic

stress-strain theory for cohesionless soil, American Society of Civil Engineers, Journal of the Geotechnical Division, GT10, pp. 1037～1053, 1975.
14) Tatsuoka, F. and K. Ishihara: Yielding of sand in triaxial compression, Soils and Foundations, Vol. 14, No. 2, pp. 63～76, 1974.
15) Miyamori, T.: Deformation and strength of sand in three dimensional stress state, Proceedings of Japan Society of Civil Engineers, No. 255, pp. 81～91, 1976 (in Japanese).
16) Yamada, Y. and K. Ishihara: Anisotropic deformation characteristics of sand under three dimensional stress conditions, Soils and Foundations, Vo . 19, No. 2, pp. 79～94, 1979.
17) Haruyama, M.: Anisotropic deformation-strength characteristics of an assembly of spherical particles under three dimensional stresses, Soils and Foundations, Vol. 21, No. 4, pp. 41～55, 1981.
18) Mróz, Z., V. A. Norris and O. C. Zienkiewicz: Application of an anisotropic hardening model in the analysis of elasto-plastic deformation of soils, Geotechnique, Vo . 29, No. 1, pp. 1～34, 1979.
19) Lade, P. V.: Elasto-plastic stress-strain theory for cohesionless soil with curved yield surfaces, International Journal of Solids and Structures, Vol. 13, pp. 1019～1035, 1977.
20) Vermeer, P. A.: A double hardening model for sand, Geotechnique, Vol. 28, No. 4, pp. 413～433, 1978.
21) Nishi, K. and Y. Esashi: Stress-strain relationships of sand based on elasto-plasticity theory, Proceedings of Japan Society of Civil Engineers, No. 280, pp. 111～122, 1978.
22) Molenkamp, F.: An elasto-plastic double hardening model (MONOT), Delft Soil Mechanics Laboratory, OC-218595, 1980.
23) Pande, G. N. and O. C. Zienkiewicz: Soil Mechanics—transient and cyclic loads, John Wiley & Sons, 1982.
24) Ishihara, K. and S. Okada: Yielding of overconsolidated sand and liquefaction model under cyclic stresses, Soils and Foundations, Vol. 18, pp. 57～72, 1978.
25) Nishi, K.: Elasto-plastic behaviour of saturated sand under undrained cyclic loading and its constitutive equation, Proceedings of Japan Society of Civil Engineers, No. 319, pp. 115～128, 1982 (in Japanese).
26) Miura, T. and N. Yamamoto: Yielding characteristics of a sand in regions of particle-crushing, Proc. 16th Annual Meeting of JSSMFE, pp. 513～516, 1981 (in Japanese).
27) Prager, W.: Recent developments in the mathematical theory of plasticity, Journal of Applied Physics, Vol. 20, pp. 235～241, 1949.
28) Hill, R.: The Mathematical Theory of Plasticity, Oxford Press, 1950.
29) Koiter, W. T.: Stress-strain relations, uniqueness and variational theorems for elastic-plastic materials with a singular yield surface, Quartly Applied Mathematics, Vol. 11, pp. 350～354, 1953.
30) Drucker, D. C. and W. Prager: Soil mechanics and plastic analysis or limit design, Quartly Applied Mathematics, Vol. 10, pp. 157～165, 1952.
31) Hirai, H. and M. Satake: Proposal of a yield function and description of plastic behavior of soft rocks, Proceedings of Japan Society of Civil Engineers, No. 320, pp. 159～164, 1982.
32) Moroto, Y.: Recoverable behaviour of sand, Soils and Foundations, Vol. 12, No. 3, pp. 65–74, 1972 (in Japanese).
33) Hirai, H., E. Yanagisawa and M. Satake: An Elastic-Plastic Constitutive Model of Soils and Rocks and Its Application to the Finite Element Analysis, Proceedings of Japan Society of Civil Engineers, No. 339, pp. 207–217, 1983.

(Received June 9, 1983)

土木学会論文報告集 第343号

砂に関する種々の弾塑性構成モデルの適用性について

(平井弘義／柳沢栄司／佐武正雄)

昭和59年3月

砂の非線形な応力-ひずみ関係については実験・理論的に数多くの研究がなされてきている．まず Roscoe を始めとする Cambridge 学派の人々によって Cam clay モデルと修正 Cam clay モデルが提案され，それらの関連流動則に基づいた構成式は土の構成モデルの端緒として多くの有益な知見を与えた．一方実験・現象の多様化に伴い，上記のモデルでは説明し得ない事実が生じ，このためより正確な土の構成式の確立が非関連流動則に基づいてなされてきている．しかしながら非関連流動則に基づく構成式については種々の提案式が見受けられ，それらの適用性に対して統一的な議論が十分なされていないように思われる．それゆえ構成式に含まれる降伏関数，塑性ポテンシャルおよび硬化パラメーターについて実験事実を踏まえて詳細な検討を行い，それらの組合せから成る種々の構成モデルについて考察を行うことは有限要素法や境界要素法などによる計算方法を有意義なものに発展させるためにも緊急な課題であると考えられる．

本研究は適用性があると考えられる7つの構成モデルを取り上げ，それらより導かれる弾塑性構成式と砂の実験結果を比較検討しそれぞれのモデルの有用性について考察を行うものであり，特に Koiter による関連流動則を非関連流動則に拡張した構成式が用いられている．7つのモデルのうちモデル (a) においては関連流動則が適用され，モデル(b)には非関連流動則が用いられており，関連および非関連流動則の有用性が検討されている．これらの2つのモデルは三軸圧縮・伸張試験における単調載荷時の塑性挙動は適切に表わすことができるが，応力経路の方向が変化する場合には適用できない欠点がある．この点を補うために，(c), (d), (e), (f) および (g) の5つのモデルが提案されている．これら5つのモデルから得られる構成式は2つ以上の関連あるいは非関連流動則を結びつけた形を呈しており，応力経路が折れ曲がるような場合にもその力学特性を表現でき得るような特徴がある．特にモデル (f) については実験事実を十分考慮した降伏関数と塑性ポテンシャルを取り入れており，簡潔な形ながら実験結果を適切に記述し得ると考えられる．一方，硬化パラメーターについては体積変形およびせん断変形に関与するそれぞれの塑性仕事に基づいた表示式が提案されており，この式は7つのモデルのすべてに適用されている．

実験においては砂の三軸圧縮・伸張試験が行われ，構成モデルの中の降伏関数，塑性ポテンシャルおよび硬化パラメーターに含まれる材料定数が求められ，それぞれのモデルの適用性が検討されている．さらに三主応力がすべて異なる一般応力状態における応力-ひずみ関係については，π 平面内における応力状態を表わす b 値のみの関数として材料定数を仮定する．このような場合，三軸圧縮および伸張試験より得られる実験結果は一般の b 値＝一定試験における2つの極限状態に相当し，b 値を変えた場合の応力-ひずみ関係が提案された構成モデルを用いて導かれている．

最後に本研究のおもな結果を要約すると次のようになる．

(1) 砂の塑性挙動を記述するために，降伏関数，塑性ポテンシャルおよび硬化パラメーターから成る7つの土のモデルが提案された．

(2) 7つのモデルより関連および非関連流動則に基づく増分形の応力-ひずみ関係式が Koiter の理論を拡張することによって得られた．

(3) それぞれのモデルの適用性が三軸圧縮・伸張試験結果との比較検討により明らかにされた．

(4) 非関連流動則は関連流動則に比べてより適切に実験結果を表わし得る．

(5) 4つのモデル(d), (e), (f) および (g) から導かれた構成式は実験結果をかなりよく表現し得る．

(6) 特にモデル(f)は既往の実験事実を十分考慮に入れた簡潔な形となっており，実験結果を適切に記述し得ると考えられる．

(7) 三主応力の異なる一般応力状態における応力-ひずみ関係が材料定数の b 値依存性を仮定することによって導かれた．